Earth and Space Science

RESEARCH ARTICLE
10.1029/2024EA003668

Worldwide Rocket Launch Emissions 2019: An Inventory for Use in Global Models

Tyler F. M. Brown[1], Michele T. Bannister[1], Laura E. Revell[1], Timofei Sukhodolov[2], and Eugene Rozanov[2,3]

[1]Te Kura Matū School of Physical and Chemical Sciences, University of Canterbury, Christchurch, New Zealand, [2]Physikalisch-Meteorologisches Observatorium Davos and World Radiation Center, Davos, Switzerland, [3]Institute for Atmospheric and Climate Science, ETH Zurich, Zurich, Switzerland

Key Points:

- We compile a comprehensive emissions inventory of all rocket launches in 2019 at 18 active spaceports
- It itemizes chemically and radiatively active species that are produced by the main rocket fuels (kerosene, cryogenic, solid and hypergolic)
- We discuss the inventory's uncertainties and its usage in global models to study the impacts of rocket launches on the ozone layer

Correspondence to:

M. T. Bannister and L. E. Revell,
michele.bannister@canterbury.ac.nz;
laura.revell@canterbury.ac.nz

Citation:

Brown, T. F. M., Bannister, M. T., Revell, L. E., Sukhodolov, T., & Rozanov, E. (2024). Worldwide rocket launch emissions 2019: An inventory for use in global models. *Earth and Space Science*, *11*, e2024EA003668. https://doi.org/10.1029/2024EA003668

Received 27 MAR 2024
Accepted 29 SEP 2024

Author Contributions:

Conceptualization: Michele T. Bannister, Laura E. Revell
Data curation: Tyler F. M. Brown
Formal analysis: Tyler F. M. Brown
Investigation: Tyler F. M. Brown
Methodology: Tyler F. M. Brown, Michele T. Bannister
Software: Tyler F. M. Brown
Supervision: Michele T. Bannister, Laura E. Revell
Validation: Tyler F. M. Brown
Visualization: Tyler F. M. Brown, Michele T. Bannister, Laura E. Revell
Writing – original draft: Tyler F. M. Brown, Michele T. Bannister, Laura E. Revell
Writing – review & editing: Tyler F. M. Brown, Michele T. Bannister, Laura E. Revell, Timofei Sukhodolov, Eugene Rozanov

Abstract The rate of rocket launches is accelerating, driven by the rapid global development of the space industry. Rocket launches emit gases and particulates into the stratosphere, where they impact the ozone layer via radiative and chemical processes. We create a three-dimensional per-vehicle inventory of stratospheric emissions, accounting for flight profiles and all major fuel types in active use (solid, kerosene, cryogenic and hypergolic). In 2019, stratospheric (15–50 km) rocket launch emissions were 5.82 Gg CO_2, 6.38 Gg H_2O, 0.28 Gg black carbon, 0.22 Gg nitrogen oxides, 0.50 Gg reactive chlorine and 0.91 Gg particulate alumina. The geographic locations of launch sites are preserved in the inventory, which covers all active launch sites in 2019. We also report the emissions data from contemporary vehicles that were not launched in 2019, so that users have freedom to construct their own launch activity scenarios. A subset of the inventory—stratospheric emissions for successful launches in 2019—is freely available and formatted for direct use in global chemistry-climate or Earth system models.

Plain Language Summary Many governments and companies have expressed bold ambitions to grow their presence in space. However, rocket launches throw out a stream of air pollutants from their burnt fuel as they pass through the stratosphere, which is where the protective ozone layer resides. Currently, launch operators do not have to measure the impacts of their activities on the ozone layer. We gather together all the publicly available information on rocket launches in 2019, from 18 active spaceports worldwide, and make some careful assumptions to convert each rocket's fuel to its burnt fuel products left in the atmosphere. We encourage modeling groups to use our inventory for studies on how rocket launches may impact the ozone layer.

1. Introduction

Rocket launches lofting payloads to orbit inject gases and particulates into the atmosphere, including the stratosphere (approximately 15–50 km), where the ozone layer resides. Stratospheric ozone absorbs harmful solar UV-B radiation and is thus essential for protection of the biosphere. In the troposphere, emission products are quickly removed by mixing, precipitation, and/or chemical oxidation. In contrast, stratospheric gases and particulates, such as from volcanoes, wildfires or anthropogenic chlorofluorocarbons, are long-lived and can be destructive to the ozone layer (Evan et al., 2023; Molina & Rowland, 1974; Randel et al., 1995; Solomon et al., 2023). Furthermore, gases and particulates in the stratosphere can have widespread effects, as the stratosphere is longitudinally well-mixed.

While natural events are singular and transient, rocket launches, though individually smaller, are made far more frequently. The last decade has witnessed 4.8% year-over-year growth in the rate of rocket launches, as commercial entities take a greater role in the expanding global space industry; as of early 2024, 26 launch providers were active (McDowell, 2022). Within this, the year 2019 was a crucial turning point for space travel, as the industry entered a "hockey stick"-like shift in the frequency of orbital launch rates around this time. Aside from the pause in launches that occurred during the onset years of the COVID-19 pandemic, this has only accelerated throughout 2024. Therefore, 2019 serves as a useful point in time to consider both the impact of present-day trends and projected future trends.

Understanding the future impacts of the launch industry in terms of fuel choices, emissions profiles, and launch cadence is increasingly important as the industry diversifies and grows. We review these aspects in Brown et al. (2023). Depending on the launch vehicle and fuel type, rocket launch exhaust can include black carbon,

alumina, nitrogen oxides ($NO_x = NO + NO_2$), reactive chlorine ($Cl_x = Cl + ClO$), carbon dioxide (CO_2), and water vapor (see Table 1; also e.g., Brown et al., 2023, Dallas et al., 2020). These species are all either radiatively active and/or contribute to ozone destruction via chemical reactions (Carpenter et al., 2018; Crutzen, 1970; Danilin, Shia, et al., 2001; Mills et al., 2008; Molina & Rowland, 1974; Morgenstern et al., 2017; Portmann et al., 2012; Revell et al., 2012; Solomon, 1999; Tian et al., 2009; Yu et al., 2019). We discuss these impacts further in Section 1.1.

As the launch industry scales up in the 2020s and the coming decades, there is a pressing need to understand the impacts of launch emissions on stratospheric ozone, as they are currently under-studied (Daniel & Reimann, 2022; Ross & Jones, 2022). The World Meteorological Organization's Scientific Assessment of Ozone Depletion (2022) noted "heightened concerns" about the impacts of an increased frequency of rocket launches on 21st century stratospheric ozone (Daniel & Reimann, 2022). Many studies to date have focused on the various impacts of only single-fuel emissions or single-species effects, and often from limited injection sites (Danilin, Ko, & Weisenstein, 2001; Danilin, Shia, et al., 2001; Jackman et al., 1996, 1998; Karol et al., 1992; Larson et al., 2017; Maloney et al., 2022; Popp et al., 2002; Prather et al., 1990; Ross et al., 2000, 2004, 2010; Voigt et al., 2013). With an eye to the future, many of the modeling studies noted above trialled much larger launch and return frequencies than were occurring at that time. This is useful in exploring the uncertain range of impacts that future launches may have on stratospheric ozone and climate. Such research was highlighted as a "Key Research Need" by the 11th Ozone Research Managers Meeting (2021). The WMO's Scientific Assessment of Ozone Depletion (2022) also noted that further research into the rapid growth of rocket launches and the impacts of their fuels on stratospheric ozone is warranted (Daniel & Reimann, 2022).

To facilitate further studies by the community and make it possible to identify any effects of the current distribution of spaceports and fuel types on stratospheric ozone, we have developed an inventory of emissions products from vehicles in use at active spaceports, as of 2019 (Section 2). Our inventory is a comprehensive snapshot of 2019's entire worldwide activity: it assesses all launch vehicles (whether they launched successfully or not), all available flight profiles, and all of the major emissions products. A subset of the inventory—rocket emissions from successful launches through the stratosphere that took place in 2019—is provided here in the standard modeling input netCDF format, intended for use by global models to simulate the impacts of rocket launch emissions on stratospheric ozone (Brown, 2024).

1.1. Impacts of Rocket Emissions on Stratospheric Ozone

CO_2 and water vapor represent the largest mass-wise component of exhaust for the launch vehicles active in 2019 (Figure 1). Both lead to radiative cooling of the stratosphere, which changes the rate of temperature-dependent ozone production and destruction reactions, such that ozone abundances increase (Dhomse et al., 2018; Portmann et al., 2012). In addition, hydrogen oxides produced from water vapor oxidation contribute to ozone loss in the stratosphere (Tian et al., 2009). As well as influencing ozone concentrations, CO_2 and water vapor contribute to climate change: Ross and Sheaffer (2014) analytically estimated a 16 mW m^{-2} radiative forcing from rocket emissions, with a 2% contribution from water vapor, while the CO_2 contribution was negligible. Black carbon and alumina exerted a larger radiative forcing, at 70% and 28%, respectively.

Alumina particles from solid rocket motors (SRMs) efficiently scatter shortwave solar irradiance and absorb in the longwave (Dykema et al., 2016). They also indirectly contribute to ozone depletion by acting as a surface medium for chlorine activation (Molina et al., 1997). Alumina particles provide sites to catalyze the $ClONO_2 + HCl \rightarrow HNO_3 + Cl_2$ reaction. However, the uptake coefficients of HCl and $ClONO_2$ are poorly constrained for stratospheric conditions and require additional laboratory measurements. In addition, the behavior of alumina particles in the stratosphere is likely affected by full or partial coating by sulfate aerosols, subject to particle sizes and background sulfate amounts (Murphy et al., 2023; Weisenstein et al., 2015).

The contribution of chlorine to ozone loss is well established from the historical use of CFCs (Molina & Rowland, 1974). Chlorine-induced ozone loss is most pronounced in spring in polar regions, when heterogeneous reactions on polar stratospheric clouds during winter lead to a build-up of Cl_2 that is subsequently photolyzed, initiating widespread ozone losses (Farman et al., 1985; Solomon, 1999). The destructive power of rocket-based chlorine has been verified by in-situ measurement of vehicle plumes (Ross et al., 2000). Other simulations focused on global impacts: a 0.4% (12 pptv) increase in background chlorine concentration yielded a 0.14% ozone

Table 1
Propellant Types and Emission Products

Fuel type	Components	Emission products	Prevalence (2019 total propellant mass burned)
Rocket Fuel Types			
Kerosene	RP-1 (Kerosene)/LOx	CO_2, H_2O, NO_x, black carbon	48%
Cryogenic	LH_2/LOx	H_2O, H_2, NO_x	6%
Solid	Al/NH_4ClO_4 & HTPB	HCl, H_2O, CO_2, NO_x, Al_2O_3, black carbon	16%
Hypergolic	N_2H_4/UDMH & N_2O_4	H_2O, N_2, CO_2, NO_x, black carbon	30%

Note. Relative prevalence is shown as a percentage of total rocket propellant mass in 2019, calculated from the emissions data presented in Table 2 and launch frequencies shown in Figure 1. SRM-emitted HCl is rapidly converted into Cl_2, which forms reactive chlorine (Cl_x).

decrease in the upper stratosphere at northern mid to high latitudes near injection sites (Jackman et al., 1996). A 0.05% polar column ozone decrease was also observed. The scenario used by Jackman et al. (1996) encompassed relatively few launches (12 large vehicles per year), suggesting that chlorine-based effects could lead to larger stratospheric ozone losses with increased launch frequencies. In a recent study examining the effects of sustained growth in rocket launch emissions from a set of vehicles in use in 2019, global-mean stratospheric ozone decreased by 0.012%. A 0.15% (1.8 ppt) increase in inorganic chlorine was responsible for almost half of the ozone loss (Ryan et al., 2022).

Both reactive chlorine and alumina particulates are emitted together in SRM exhaust wakes, compounding the ozone losses that occur (Danilin, Ko, & Weisenstein, 2001). Expanding globally, this effect was demonstrated by Jackman et al. (1998) using 2-D photochemistry transport models through infrequent launch scenarios of SRM-equipped vehicles. Annual average global ozone decreased by 0.025%, due to both alumina particulates and chlorine chemistry acting in tandem. Of particular importance in assessing alumina-driven destruction of ozone is particle size: only the sub-micron fraction of alumina in the stratosphere contributes to regional chemical processes because particles larger than 1 μm are efficiently removed by gravitational sedimentation (Ross & Sheaffer, 2014; Schmid et al., 2003). While the total alumina amount is well-understood for SRM emission, particle size distributions are not. Future studies should revisit the sensitivity of stratospheric ozone to sub-micron alumina from SRMs, given planned launches. The ablation of re-entering rocket parts, space debris and deorbiting satellite constellations will provide another source of sub-micron alumina, as well as other exotic metals; these yet-to-be-understood effects should also be examined (Boley & Byers, 2021; Murphy et al., 2023; S.-H. Park et al., 2021).

Another product of spacecraft and space debris re-entry is NO_x, which is emitted by all four types of rocket propellants included in our inventory. Re-entry NO_x is not included here, because data are unavailable for many currently-used vehicles. Anthropogenic NO_x, which typically enters the stratosphere following photochemical breakdown of nitrous oxide (N_2O), destroys ozone via gas-phase catalytic ozone loss cycles (Ravishankara et al., 2009; Revell et al., 2012). Ross et al. (2004) found that for a launch scenario of 10 hypergolic-fueled Proton vehicles per year, the steady-state ozone loss predicted is small, at 1.2×10^{-4}% per year, associated with NO_x emissions. A 20% decrease in column ozone in the immediate rocket plume was identified, which recovered due to atmospheric mixing. However, NO_x abundances in rocket exhaust are significantly smaller than those produced upon spacecraft and space debris atmospheric re-entry (Popp et al., 2002). The study by Ryan et al. (2022) on 2019 rocket launches and re-entry considers ablative NO_x production and shows that re-entry NO_x can have a significant effect on stratospheric ozone. For launch scenarios considering re-entry NO_x production, a 0.5% loss of global average column ozone was seen, with polar losses exceeding 2% (Larson et al., 2017).

Finally, black carbon is emitted by both liquid and solid rocket fuels. Black carbon contributes to ozone destruction and climate warming, mainly due to its longevity and warming effects, since it is a strong absorber of both longwave and shortwave radiation (Ban-Weiss et al., 2012; Kravitz et al., 2012; Mills et al., 2008). In a recent modeling study, a constant annual black carbon emission of 10 Gg yr^{-1} was injected into the stratosphere at a single latitude (30°N). Persistent levels of black carbon were observed after 4–6 years of rocket launch activity, with year-round ozone loss of 5–15 DU in the Northern Hemisphere and a potentially more severe Antarctic ozone hole (Maloney et al., 2022). Simulations with stratospheric black carbon emission of 0.6 Gg yr^{-1} show a 1% depletion in tropical stratospheric ozone and 6% in polar stratospheric ozone (Ross et al., 2010).

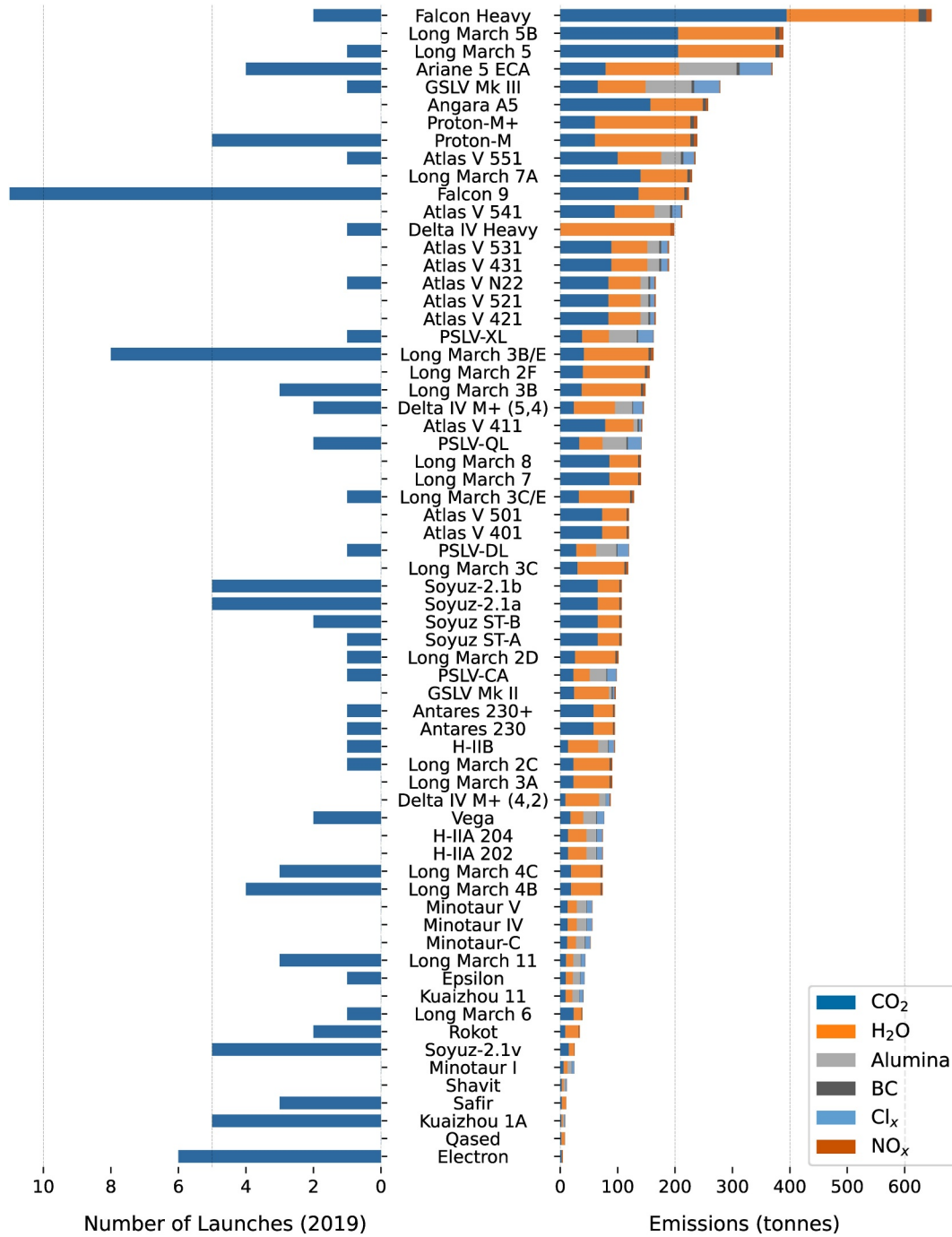

Figure 1. Total stratospheric emissions (within 15–50 km altitude) of each launch vehicle in tonnes. Colors represent individual emission products (right), and 2019 launch frequencies are shown on the left. Total emissions are a function of vehicle propellant mass, and do not necessarily map to ozone impact.

2. Inventory Development

2.1. Vehicles

We compile a comprehensive inventory of current launch vehicles and their stratospheric emissions contributions by mass (Tables 2–6). In total, the inventory includes 65 vehicles from 11 launcher families, including alternate configurations and contemporary counterparts, for 97 successful launches made in 2019. Data are taken from the

Table 2
Inventory of Stratospheric Emissions (Within 15–50 km Altitude) per Emission Species

Vehicle	CO_2	H_2O	Black carbon	NO_x	Cl_x	Alumina
Angara A5	157.08	91.63	5.24	3.67	0	0
Antares 230	58.08	33.88	1.94	1.36	0	0
Antares 230+	58.08	33.88	1.94	1.36	0	0
Ariane 5 ECA	79.09	128.14	5.27	1.8	55.36	100.18
Atlas V 401	73.05	42.61	2.44	1.7	0	0
Atlas V 411	78.46	49.29	2.8	1.76	3.79	6.85
Atlas V 421	83.87	55.96	3.16	1.81	7.58	13.71
Atlas V 431	89.28	62.63	3.52	1.87	11.36	20.56
Atlas V 501	73.05	42.61	2.44	1.7	0	0
Atlas V 521	83.87	55.96	3.16	1.81	7.58	13.71
Atlas V 531	89.28	62.63	3.52	1.87	11.36	20.56
Atlas V 541	94.69	69.31	3.88	1.92	15.15	27.41
Atlas V 551	100.11	75.98	4.24	1.98	18.94	34.27
Atlas V N22	83.87	55.96	3.16	1.81	7.58	13.71
Delta IV M+ (4,2)	8.91	59.09	0.59	1.68	6.24	11.29
Delta IV M+ (5,4)	23.76	71.74	1.58	1.64	16.63	30.1
Delta IV Heavy	0	191.96	0	6.33	0	0
Electron	2.66	1.55	0.09	0.06	0	0
Epsilon	9.89	12.19	0.66	0.1	6.92	12.52
Falcon 9	136.58	79.67	4.55	3.19	0	0
Falcon Heavy	394.56	230.16	13.15	9.21	0	0
GSLV Mk II	24.12	60.83	2.29	2.09	2.53	4.58
GSLV Mk III	65.28	83.59	4.42	0.84	44.28	80.13
H-IIA 202	13.65	32	0.91	0.64	9.56	17.29
H-IIA 204	13.65	32	0.91	0.64	9.56	17.29
H-IIB	13.65	52.4	0.91	1.31	9.56	17.29
Kuaizhou 1A	2.03	2.5	0.14	0.02	1.42	2.57
Kuaizhou 11	9.45	11.66	0.63	0.09	6.62	11.97
Long March 11	10.2	12.58	0.68	0.1	7.14	12.92
Long March 2C	22.97	63.17	2.3	2.3	0	0
Long March 2D	25.69	70.66	2.57	2.57	0	0
Long March 2F	39.39	108.33	3.94	3.94	0	0
Long March 3A	22.91	62.99	2.29	2.29	0	0
Long March 3B	37.53	103.2	3.75	3.75	0	0
Long March 3B/E	41.07	112.95	4.11	4.11	0	0
Long March 3C	29.9	82.23	2.99	2.99	0	0
Long March 3C/E	32.47	89.3	3.25	3.25	0	0
Long March 4B	18.72	51.48	1.87	1.87	0	0
Long March 4C	18.72	51.48	1.87	1.87	0	0
Long March 5	205.63	169.54	6.85	6.43	0	0
Long March 5B	205.63	169.54	6.85	6.43	0	0
Long March 6	23.45	13.68	0.78	0.55	0	0
Long March 7	85.68	49.98	2.86	2	0	0

Table 2
Continued

Vehicle	CO_2	H_2O	Black carbon	NO_x	Cl_x	Alumina
Long March 7A	140.04	81.69	4.67	3.27	0	0
Long March 8	85.68	49.98	2.86	2	0	0
Minotaur I	5.71	7.05	0.38	0.06	4	7.24
Minotaur IV	13.05	16.09	0.87	0.13	9.13	16.53
Minotaur V	13.05	16.09	0.87	0.13	9.13	16.53
Minotaur-C	12.31	15.18	0.82	0.12	8.62	15.59
Pegasus-XL	3.22	3.97	0.21	0.03	2.25	4.07
Proton-M	60.47	166.28	6.05	6.05	0	0
Proton-M+	60.47	166.28	6.05	6.05	0	0
PSLV-CA	22.96	28.32	1.53	0.23	16.07	29.09
PSLV-DL	27.99	34.53	1.87	0.28	19.6	35.46
PSLV-QL	33.03	40.73	2.2	0.33	23.12	41.83
PSLV-XL	38.06	46.94	2.54	0.38	26.64	48.21
Qased	2.03	5.59	0.2	0.2	0	0
Rokot	8.57	23.58	0.86	0.86	0	0
Safir	2.57	7.07	0.26	0.26	0	0
Shavit	2.7	3.33	0.18	0.03	1.89	3.42
Soyuz ST-A	65.25	38.06	2.18	1.52	0	0
Soyuz ST-B	65.25	38.06	2.18	1.52	0	0
Soyuz-2.1v	15.12	8.82	0.5	0.35	0	0
Soyuz-2.1a	65.25	38.06	2.18	1.52	0	0
Soyuz-2.1b	65.25	38.06	2.18	1.52	0	0
Vega	17.93	22.12	1.2	0.18	12.55	22.71

Note. All quantities are given in metric tons. Vehicles are listed alphabetically.

references listed in Data Availability Statement. We define our volume of interest as altitudes of 15–50 km; these altitudes are where data are consistently available. For ease of comparison, we distinguish vehicles similarly to how they are distinguished by launch providers: by generational design, booster configuration, payload configuration, and launch location. The first two aspects alter propellant mass—and thus emission mass—considerably. Comparatively, vehicles which have multiple launch locations, such as the Soyuz vehicle, or configurations in which only the top-most payload fairing size is altered, such as some Atlas IV vehicles, demonstrate identical stratospheric emission, as neither characteristic affects our volume of interest. Two vehicles from 2019, Jielong 1 and Hyperbola-1, are omitted from the data set as insufficient information is publicly and reliably available. The inventory also includes some contemporary vehicles or configurations which were not launched in 2019, for comparison or inclusion in modeling, if desired; these are not in the netCDF file described in Section 3. We include these vehicles in our inventory tables as they were launched in recent years, albeit not 2019. Researchers wishing to study the impacts of these vehicles on the atmosphere are able to add data from Tables 2–6 for those vehicles to the netCDF file.

We include launches here if they emitted products into the altitude range that we consider (Section 2.2). This means two launches that did not reach their target orbit are included in this data set: a Long March 4C (22 May 2019) launch and a Vega vehicle (11 July 2019) launch. The vehicle malfunctions for both these launches were at altitudes above our volume of interest, and thus they still contribute to stratospheric emissions. For the whole vehicle set, launch emissions are then calculated on a per-vehicle basis, using their successful launches in 2019 as the reference year (McDowell, 2022).

Table 3
Vehicle Information for the Emissions Inventory

Vehicle	Family	Country	Launch site(s)
Angara A5	Angara	Russia	Plesetsk
Antares 230	Antares	USA	Wallops
Antares 230+	Antares	USA	Wallops
Ariane 5	ECA Ariane	Europe	Kourou
Atlas V 401	Atlas	USA	Cape Canaveral, Vandenberg
Atlas V 411	Atlas	USA	Cape Canaveral, Vandenberg
Atlas V 421	Atlas	USA	Cape Canaveral, Vandenberg
Atlas V 431	Atlas	USA	Cape Canaveral, Vandenberg
Atlas V 501	Atlas	USA	Cape Canaveral, Vandenberg
Atlas V 521	Atlas	USA	Cape Canaveral, Vandenberg
Atlas V 531	Atlas	USA	Cape Canaveral, Vandenberg
Atlas V 541	Atlas	USA	Cape Canaveral, Vandenberg
Atlas V 551	Atlas	USA	Cape Canaveral, Vandenberg
Atlas V N22	Atlas	USA	Cape Canaveral, Vandenberg
Delta IV M+ (4,2)	Delta	USA	Cape Canaveral, Vandenberg
Delta IV M+ (5,4)	Delta	USA	Cape Canaveral, Vandenberg
Delta IV Heavy	Delta	USA	Cape Canaveral, Vandenberg
Electron	Electron	NZ	Māhia
Epsilon	Epsilon	Japan	Uchinoura
Falcon 9	Falcon	USA	Cape Canaveral, Vandenberg
Falcon Heavy	Falcon	USA	Cape Canaveral
GSLV Mk II	GSLV	India	Satish Dawan
GSLV Mk III	GSLV	India	Satish Dawan
H-IIA 202	H-II	Japan	Tanegashima
H-IIA 204	H-II	Japan	Tanegashima
H-IIB	H-II	Japan	Tanegashima
Kuaizhou 1A	Kuaizhou	China	Jiuquan, Taiyuan
Kuaizhou 11	Kuaizhou	China	Jiuquan, Taiyuan
Long March 11	Long March	China	Jiuquan, Xichang, Yellow Sea
Long March 2C	Long March	China	Jiuquan, Taiyuan, Xichang
Long March 2D	Long March	China	Jiuquan, Taiyuan, Xichang
Long March 2F	Long March	China	Jiuquan
Long March 3A	Long March	China	Xichang
Long March 3B	Long March	China	Xichang
Long March 3B/E	Long March	China	Xichang
Long March 3C	Long March	China	Xichang
Long March 3C/E	Long March	China	Xichang
Long March 4B	Long March	China	Jiuquan, Taiyuan
Long March 4C	Long March	China	Jiuquan, Taiyuan, Xichang
Long March 5	Long March	China	Wenchang
Long March 5B	Long March	China	Wenchang
Long March 6	Long March	China	Taiyuan
Long March 7	Long March	China	Wenchang

Table 3
Continued

Vehicle	Family	Country	Launch site(s)
Long March 7A	Long March	China	Wenchang
Long March 8	Long March	China	Wenchang
Minotaur I	Minotaur	USA	Vandenberg, Wallops
Minotaur IV	Minotaur	USA	Cape Canaveral, Vandenberg, Wallops
Minotaur V	Minotaur	USA	Vandenberg, Wallops
Minotaur-C	Minotaur	USA	Vandenberg
Pegasus-XL	Pegasus	USA	Cape Canaveral
Proton-M	Proton	Russia	Baikonur
Proton-M+	Proton	Russia	Baikonur
PSLV-CA	PSLV	India	Satish Dawan
PSLV-DL	PSLV	India	Satish Dawan
PSLV-QL	PSLV	India	Satish Dawan
PSLV-XL	PSLV	India	Satish Dawan
Qased	Qased	Iran	Semnan
Rokot	Rokot	Russia	Plesetsk, Baikonur
Safir	Safir	Iran	Semnan
Shavit	Shavit	Israel	Palmachin
Soyuz ST-A	Soyuz	Russia	Kourou
Soyuz ST-B	Soyuz	Russia	Kourou
Soyuz-2.1v	Soyuz	Russia	Plesetsk, Baikonur, Vostochny
Soyuz-2.1a	Soyuz	Russia	Plesetsk, Baikonur, Vostochny
Soyuz-2.1b	Soyuz	Russia	Plesetsk, Baikonur, Vostochny
Vega	Vega	Europe	Kourou

2.2. Rocket Launch Emissions

By mass, the most common emissions are gas-phase products (carbon dioxide, water vapor, NO_x and reactive chlorine, Figure 1). Emissions for these products are compiled as described below. Additional considerations are required for the particulates black carbon and alumina, which are described in Sections 2.3 and 2.4.

For each vehicle, we calculate the propellant mass of the rocket stages burning to 50 km altitude to produce the mass of their experimentally measured exhaust byproducts, using an emission index. Emissions above 50 km are modeled as exponential decay, as described in Section 2.5. Vehicle propellant mass is multiplied by the emission index to yield emission mass at each kilometer. This emission index is represented as grams of exhaust byproduct per kilogram of vehicle propellant, g kg^{-1} (Table 8). Our emission index values are sourced from previous studies per Ross and Sheaffer (2014), Desain and Brady (2014), Larson et al. (2017), Maloney et al. (2022), Ryan et al. (2022), and Pradon et al. (2023). We consider emission mass injected within 15–50 km altitude in calculating stratospheric vehicle emissions, as shown in Table 2. Note that the netCDF file provided for modeling studies (Section 3) contains emissions starting at ground level; however, emissions in the oxygen-rich troposphere are quickly removed by secondary combustion and washout, and are not relevant for studies on stratospheric ozone.

For most vehicles, often only the first stage and optional booster stages create relevant emissions. The full list of references for the fuel type, propellant mass, and flight profile estimates for all relevant launch stages are provided in Section 5. Vehicles which use UH25 SRM (SRM) propellant (vs. the common UDMH) are handled similarly to Desain and Brady (2014) by adjusting the emission index to represent different mixture proportions. For some vehicles, data are unavailable concerning their total propellant mass, propellant mixing ratio and/or flight profile

Table 4
Unprocessed Main Stages Source Data for the Emissions Inventory

Vehicle	Fuel type	Total propellant mass (kg)	Mixing ratio (kg/kg)
Angara A5	Kerosene	132,600	2.6
Antares 230	Kerosene	242,000	2.6
Antares 230+	Kerosene	242,000	2.6
Ariane 5 ECA	Cryogenic	170,000	6.1
Atlas V 401	Kerosene	284,089	2.72
Atlas V 411	Kerosene	284,089	2.72
Atlas V 421	Kerosene	284,089	2.72
Atlas V 431	Kerosene	284,089	2.72
Atlas V 501	Kerosene	284,089	2.72
Atlas V 521	Kerosene	284,089	2.72
Atlas V 531	Kerosene	284,089	2.72
Atlas V 541	Kerosene	284,089	2.72
Atlas V 551	Kerosene	284,089	2.72
Atlas V N22	Kerosene	284,089	2.72
Delta IV M+ (4,2)	Cryogenic	200,400	5.97
Delta IV M+ (5,4)	Cryogenic	200,400	5.97
Delta IV Heavy	Cryogenic	200,400	5.97
Electron	Kerosene	9,250	2.42*
Epsilon	Solid	65,000	0.18*
Falcon 9	Kerosene	411,000	2.3
Falcon Heavy	Kerosene	411,000	2.3
GSLV Mk II	Solid	138,200	0.18*
GSLV Mk III	Hypergolic	116,000	1.87
H-IIA 202	Cryogenic	101,100	5.9
H-IIA 204	Cryogenic	101,100	5.9
H-IIB	Cryogenic	177,800	5.9
Kuaizhou 1A	Solid	15,000*	0.18*
Kuaizhou 11	Solid	70,000*	0.18*
Long March 11	Solid	35,000	0.18*
Long March 2C	Hypergolic	162,706	2.4*
Long March 2D	Hypergolic	182,000	2.4*
Long March 2F	Hypergolic	187,000	2.4*
Long March 3A	Hypergolic	171,800	2.4*
Long March 3B	Hypergolic	171,800	2.4*
Long March 3B/E	Hypergolic	186,200	2.4*
Long March 3C	Hypergolic	171,800	2.4*
Long March 3C/E	Hypergolic	186,200	2.4*
Long March 4B	Hypergolic	182,000	2.4*
Long March 4C	Hypergolic	182,000	2.4*
Long March 5	Cryogenic	165,300	5.5
Long March 5B	Cryogenic	165,300	5.5
Long March 6	Kerosene	76,000	2.6
Long March 7	Kerosene	174,000	2.6

Table 4
Continued

Vehicle	Fuel type	Total propellant mass (kg)	Mixing ratio (kg/kg)
Long March 7A	Kerosene	174,000	2.6
Long March 8	Kerosene	174,000	2.6
Minotaur I	Solid	20,785	0.18*
Minotaur IV	Solid	45,370	0.18*
Minotaur V	Solid	45,370	0.18*
Minotaur-C	Solid	48,948	0.18*
Pegasus-XL	Solid	15,010	0.18*
Proton-M	Hypergolic	428,300	2.67
Proton-M+	Hypergolic	428,300	2.67
PSLV-CA	Solid	138,200	0.18*
PSLV-DL	Solid	138,200	0.18*
PSLV-QL	Solid	138,200	0.18*
PSLV-XL	Solid	138,200	0.18*
Qased	Hypergolic	14,400*	2.5*
Rokot	Hypergolic	71,450	2.5*
Safir	Hypergolic	18,200*	2.5*
Shavit	Solid	12,750	0.18*
Soyuz ST-A	Kerosene	90,100	2.47
Soyuz ST-B	Kerosene	90,100	2.47
Soyuz-2.1v	Kerosene	119,000	2.8
Soyuz-2.1a	Kerosene	90,100	2.47
Soyuz-2.1b	Kerosene	90,100	2.47
Vega	Solid	88,000	0.19

Note. Solid propellant mixing ratio is represented as the percentage of alumina additive. Starred entries indicate unavailable data which was inferred from vehicles with similar sizing, family, or configuration. All other values come from the available literature.

data. For these vehicles we infer unavailable data from vehicles with similar configurations, of a similar family, or a similar size, as specified in Tables 4–6.

2.3. Black Carbon

The complexity of estimating a black carbon emission index relies on current published understanding of engines with propellants that include carbon, and complex afterburning processes. Secondary combustion (afterburning) of black carbon is highly altitude-dependent, with the majority of exhaust mass consumed at lower altitudes. We adopt the black carbon estimates of Maloney et al. (2022) (20 g kg^{-1} emission index) due to their careful consideration of these processes for black carbon. We note our annual stratospheric mass of emitted black carbon differs from Maloney et al. (2022), due to different fundamental base assumptions for the global mean propellant load. Using the same estimation:

$$E_{BC} = N \times \frac{1}{2} \overline{P} \times EI(BC) \quad (1)$$

with N representing the annual amount of launches, $\overline{P}$ the global mean propellant mass, $\frac{1}{2}$ as the mass fraction of emissions at stratospheric altitudes, and $EI(BC)$ as the black carbon emission index. We use N as 97, and alter the mean propellant load $\overline{P}$ based on our inventory assessment. This lowers the $\overline{P}$ value to yield a total annual stratospheric emission of ~0.3 Gg. Table 7 lists the values for $\overline{P}$ (propellant mass across all fuel types), as both an

Table 5
Unprocessed Booster Stage Source Data (Where Applicable) for the Emissions Inventory

Vehicle	Fuel type	Total propellant mass (kg)	Mixing ratio (kg/kg)
Angara A5	Kerosene	530,400	2.6
Ariane 5 ECA	Solid	476,000	0.18
Atlas V 411	Solid	42,630	0.18*
Atlas V 421	Solid	85,260	0.18*
Atlas V 431	Solid	127,890	0.18*
Atlas V 521	Solid	85,260	0.18*
Atlas V 531	Solid	127,890	0.18*
Atlas V 541	Solid	170,520	0.18*
Atlas V 551	Solid	213,150	0.18*
Atlas V N22	Solid	85,260	0.18*
Delta IV M+ (4,2)	Solid	59,400	0.18*
Delta IV M+ (5,4)	Solid	118,800	0.18*
Delta IV Heavy	Cryogenic	400,800	5.97
Falcon Heavy	Kerosene	822,000	2.3
GSLV Mk II	Hypergolic	170,800	1.87
GSLV Mk III	Solid	410,000	0.18*
H-IIA 202	Solid	65,000	0.18*
H-IIA 204	Solid	65,000	0.18*
H-IIB	Solid	65,000	0.18*
Long March 11	Solid	20,000*	0.18*
Long March 2F	Hypergolic	151,200	2.4*
Long March 3B	Hypergolic	150,800	2.4*
Long March 3B/E	Hypergolic	164,400	2.4*
Long March 3C	Hypergolic	75,400	2.4*
Long March 3C/E	Hypergolic	82,200	2.4*
Long March 5	Kerosene	571,200	2.6
Long March 5B	Kerosene	571,200	2.6
Long March 7	Kerosene	151,000	2.6
Long March 7A	Kerosene	302,000	2.6
Long March 8	Kerosene	151,000	2.6
Minotaur I	Solid	6,237	0.18*
Minotaur IV	Solid	24,490	0.18*
Minotaur V	Solid	24,490	0.18*
Minotaur-C	Solid	15,101	0.18*
PSLV-DL	Solid	24,400	0.18*
PSLV-QL	Solid	48,800	0.18*
PSLV-XL	Solid	73,200	0.18*
Soyuz ST-A	Kerosene	156,640	2.47
Soyuz ST-B	Kerosene	156,640	2.47
Soyuz-2.1a	Kerosene	156,640	2.47
Soyuz-2.1b	Kerosene	156,640	2.47

Note. Solid propellant mixing ratio is represented as the percentage of alumina additive. Starred entries indicate unavailable data which was inferred from vehicles with similar sizing, family, or configuration. All other values come from the available literature.

Table 6
Flight Profile Data for the Emissions Inventory: Main Stage Start and End Altitudes and, Where Applicable, Booster Stage Start and End Altitudes

Vehicle	Main start (km)	Main end (km)	Booster start (km)	Booster end (km)
Angara A5	0	120	0	86
Antares 230	0	90	–	–
Antares 230+	0	90	–	–
Ariane 5 ECA	0	200	0	65
Atlas V 401	0	84	–	–
Atlas V 411	0	84	0	26
Atlas V 421	0	84	0	26
Atlas V 431	0	84	0	26
Atlas V 501	0	84	–	–
Atlas V 521	0	84	0	26
Atlas V 531	0	84	0	26
Atlas V 541	0	84	0	26
Atlas V 551	0	84	0	26
Atlas V N22	0	84	0	26
Delta IV M+ (4,2)	0	150	0	30
Delta IV M+ (5,4)	0	170	0	45
Delta IV Heavy	0	180	0	95
Electron	0	75	–	–
Epsilon	0	71	–	–
Falcon 9	0	65	–	–
Falcon Heavy	0	90	0	60
GSLV Mk II	40	166	0	60
GSLV Mk III	40	166	0	70
H-IIA 202	0	240	0	50
H-IIA 204	0	240	0	50
H-IIB	0	180	0	50
Kuaizhou 1A	0*	80*	–	–
Kuaizhou 11	0*	80*	–	–
Long March 11	25*	60*	0*	25*
Long March 2C	0	50	–	–
Long March 2D	0*	50*	–	–
Long March 2F	0*	70*	0*	54*
Long March 3A	0	54	–	–
Long March 3B	0	71	0	54
Long March 3B/E	0	70	0	54
Long March 3C	0	63	0	47
Long March 3C/E	0*	63*	0*	47*
Long March 4B	0*	70*	–	–
Long March 4C	0*	70*	–	–
Long March 5	0*	120*	0*	60*
Long March 5B	0*	120*	0*	60*
Long March 6	0*	70*	–	–

Table 6
Continued

Vehicle	Main start (km)	Main end (km)	Booster start (km)	Booster end (km)
Long March 7	0*	120*	0*	60*
Long March 7A	0*	120*	0*	60*
Long March 8	0*	120*	0*	60*
Minotaur I 16	55	0	16	
Minotaur IV	25*	60*	0*	25*
Minotaur V	25*	60*	0*	25*
Minotaur-C	21	61	0	21
Pegasus-XL	12	61	–	–
Proton-M	0	50	–	–
Proton-M+	0	50	–	–
PSLV-CA	0	65	–	–
PSLV-DL	0	65	0	48
PSLV-QL	0	65	0	48
PSLV-XL	0	65	0	48
Qased	0*	50*	–	–
Rokot	0	60	–	–
Safir	0*	50*	–	–
Shavit	0*	50*	–	–
Soyuz ST-A	45	170	0	45
Soyuz ST-B	45	170	0	45
Soyuz-2.1v	0	170	–	–
Soyuz-2.1a	45	170	0	45
Soyuz-2.1b	45	170	0	45
Vega	0	53	–	–

Note. Starred entries indicate unavailable data which was inferred from vehicles with similar sizing, family, or configuration. All other values come from the available references.

annual mean, and an annual mean weighted for launch frequency. These yearly propellant mass values are slightly overestimated (<10%) to account for small amounts of missing vehicle data (specified in Tables 3–6).

Table 7
Mean Propellant Mass Across All Vehicles Launched per Year From 2017 to 2022

Year	Mean propellant Mass (tonnes)	Weighted mean propellant Mass (tonnes)
2017	298	348
2018	326	331
2019	339	349
2020	337	337
2021	323	320
2022	319	333

Note. Weighted mean propellant mass includes weighting based on frequency of launches for all fuel types.

Our values for stratospheric altitudes (15–50 km) are of a comparable order of magnitude to the 1 Gg predicted by Maloney et al. (2022) for altitudes between 5 and 70 km (using a different approach to that used here, as discussed above) and the 0.5 Gg estimated by Ryan et al. (2022) (using a similar approach to us, but for all altitudes 0–80 km).

2.4. Alumina

As shown in Table 8, the alumina emission index is 380 g kg^{-1}. However, most of the alumina aerosol mass sediments rapidly out of the atmosphere. Only the sub-micron fraction of alumina (particles smaller than 1 μm in diameter) can remain suspended in the stratosphere for several years, where it is relevant for radiative forcing and ozone loss (Ross & Sheaffer, 2014; Voigt et al., 2013). The emission index of sub-micron fraction alumina depends on the particle size distribution, however, this is poorly characterized for SRMs and varies from vehicle to vehicle (Danilin, Shia, et al., 2001). Ross and Sheaffer (2014) report a range of the sub-micron fraction alumina emissions

Table 8
Emission Index (EI) for Each Emission Species

Fuel type	CO_2	H_2O	Black carbon	NO_x	Cl_x	Alumina
RP-1/LOX	600	350	20	14	0	0
LH2/LOX	0	1,000	0	33	0	0
N2O4/UH25	200	550	20	20	0	0
N2O4/UDMH	200	550	20	20	0	0
HTPB	300	370	20	3	210	380[a]

Note. All quantities are expressed as grams of exhaust species per kilogram of propellant (g kg^{-1}). [a]Refer to Section 2.4.

index as 10–120 g kg^{-1}, which they determine "reasonable," with a "likely" value of 60 g kg^{-1}. Ryan et al. (2022) assumed that 8% of alumina particles are in the sub-micron range, based on plume measurements of an Athena II SRM (Schmid et al., 2003). However, it should be noted that the Athena II rocket. along with the Titan IV and Space Shuttle rockets, on which previous estimates of the alumina particle size distribution were based (Danilin, Shia, et al., 2001), were not launched in 2019 and are not included in the inventory.

Given the large uncertainties associated with alumina, we report the emission index in Table 8 so that users have the freedom to specify their own value for submicron fraction alumina. We do however recommend that users of the inventory scale the total alumina emission index (380 g kg^{-1}) to a smaller value representative of the sub-micron fraction alumina, such as 60 g kg^{-1} as reported by Ross and Sheaffer (2014). Because the alumina particle size distribution is poorly characterized, we suggest that users map the sub-micron emissions to their model's native aerosol scheme or apply a unimodal distribution for ease of use. We note that the natural alumina influx from the input of ablated meteorites is very low (Carrillo-Sánchez et al., 2020), so quantification of the anthropogenic effects are important.

2.5. Emissions Profiles

The four principal propellant types in our catalog are kerosene-based, cryogenic (LH_2), hypergolic, and solid fuel (Table 1). We make the assumptions that upon launching from ground level, the rocket ignites, then burns its propellant mixture continuously and consistently throughout its flight until the entirety of its fuel mass is spent, and that the entirety of this burned fuel is converted to the corresponding emission products in Table 1. Due to the combustion reaction in practice burning fuel-rich, rather than in stoichiometric ratio, our assumption that all fuel is converted to exhaust products will slightly overestimate the true emissions.

We estimate a burn profile that is linear with respect to altitude, ignoring any engine throttling (which is vehicle-specific across a small set of the vehicles here) or complexity in plume modeling (Murray et al., 2013; Sheaffer, 2021). More realistic burn profiles display significant propellant mass burning rates at low altitudes, which reduce as the vehicle reaches stratospheric altitudes (Pradon et al., 2023). Our assumption will thus slightly miscount stratospheric emissions, but this effect is vehicle-dependent and not a limiting feature of the inventory. Using our linear burning assumptions, we find a ∼9% overestimate of stratospheric emissions (from all fuel types) compared to Ross and Sheaffer (2014), and an underestimate in black carbon emissions of 20% (altitude-dependent; with closer agreement above 55 km) compared with Maloney et al. (2022). This suggests that our assumptions provide a reasonable middle ground estimate for use in modeling.

The flight profile of a given rocket is unique to the launch parameters, destination orbit, and mission plan. The time spent burning fuel within stratospheric altitudes varies greatly across the vehicles listed in the inventory. However, each unique vehicle configuration generally only sees slight deviations of flight profile within its own launches. Our simplification to a linear burn profile coupled with our flight profile data (Table 6) allows for quicker generalization of per-kilometer emission mass, though we note it lacks the precision of physically calculated burn rates (e.g., Pradon et al., 2023), for a limited vehicle set).

We calculate per-kilometer emission mass from ground to 50 km. Some of the data available extends beyond this altitude. However, due to data availability constraints on some vehicles, and the reduced importance of mesospheric emissions in our study, we introduce an exponential decay above 50 km through to 80 km, to normalize the inventory across all vehicles. The mass of fuel emitted above 50 km is highly vehicle-dependent. Both the range of altitude and burn profile assumptions are points for future data set enhancement; we note the netCDF file extends to 80 km. Given that gravitational settling and mesospheric circulation will transport any aerosols released above 50 km into the upper stratosphere (Brooke et al., 2017), we are confident that an emissions cap at 80 km is appropriate for modeling launch vehicles active in 2019. If a user wishes to make a different assumption than exponential decay above 50 km through to 80 km, they are able to add data into the netCDF file above 50 km; such as if emissions data on a particular vehicle becomes publicly available in the future.

Sharp cutoffs (e.g., 45 km in Figure 2) are where either booster or main engine cutoff occur and the vehicle switches to a new burn stage. The emission mass of each species is proportional during each stage due to the

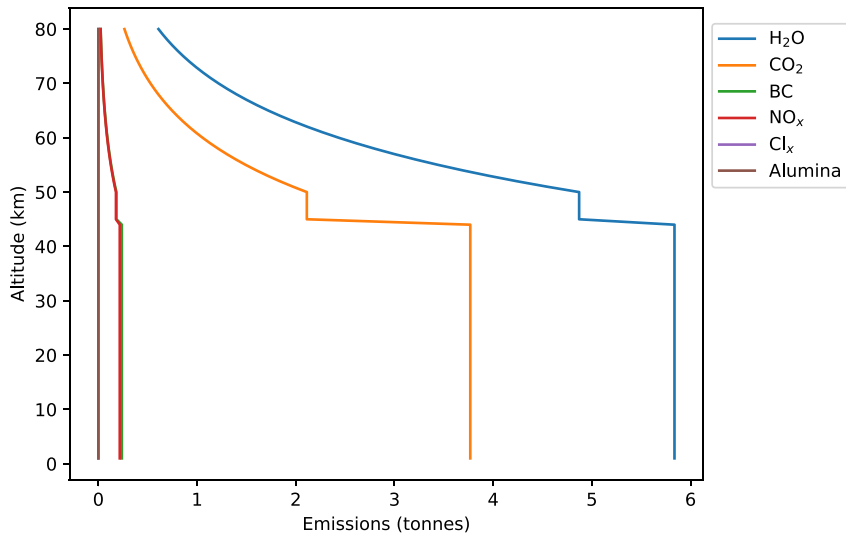

Figure 2. Example emissions profile for all launches at Baikonur Cosmodrome (Kazakhstan) in August 2019: this includes one Proton-M vehicle launch and one Soyuz 2.1a vehicle launch summed together. Emission mass is proportional to propellant burned per kilometer, representing the estimated burn profile for this site. Note that the purple and brown lines, for Cl_x and alumina respectively, overlap. For the Soyuz 2.1a, the booster engine cutoff occurs at 45 km, and the main engine then provides thrust with a lower emission production rate. The Proton-M contributes a constant emission mass over the 1–50 km range. See Table 6 for flight profile altitudes.

consistency in fuel type used. Proportionality can change at these cutoff points due to a booster or secondary stage using an alternate fuel. For tropospheric altitudes, more realistic burn rates (and thus emission mass created) can be seen in Figure 1 from Ross and Sheaffer (2014).

As a rocket launches to space, it follows a non-linear trajectory towards the desired orbital inclination, dependent on the payload's orbital destination and the location of the launch. The choice of flight profile will vary the time spent within the stratosphere. We selected median flight profiles for each vehicle from among the suite of trajectory options that operators offered, cross-referenced with diverse sources on post-launch altitude reports (note that the industry convention is to report launches in burn timing instead of altitude). Estimates from Pradon et al. (2023) have thoroughly calculated flight profiles, but do not encompass all vehicle launches or configurations represented in our inventory. No suborbital vehicles are included in our inventory, due to their poorly quantified flight profiles. Reusable rockets reserve a small amount of fuel for controlled return—we omit this edge case by assuming all propellant is burned. This behaviour only occurs for Falcon vehicles; they typically reserve <6% of total propellant mass for their stabilization burn (60–30 km) and landing burn (<5 km) (Y. Kim et al., 2021).

While re-entry ablation of depleted stages can contribute to NO_x creation, concentrated around altitudes 50 km and above (S.-H. Park et al., 2021), the amount generated is highly dependent on the component surface area, geometry, velocity, and mass (S. Kim et al., 2019). Early Space Shuttle estimates of ablative NO_x exist (C. Park & Rakich, 1980), but little data are available for newer vehicles. Due to these factors, we omit ablative NO_x contributions; our outcomes thus have lower NO_x emissions relative to those seen in other studies (Larson et al., 2017; Ryan et al., 2022).

The final inventory (Table 2) quantifies the stratospheric contributions by mass of carbon dioxide, water vapor, alumina, black carbon, NO_x, and reactive chlorine. The inventory preserves the geolocation of emissions globally, allowing the transport of emission species to be assessed (Figure 3). Figure 1 demonstrates how each vehicle contributes a unique combination of exhaust byproducts relative to its emission per launch, balanced with its launch frequency in 2019. With the exception of Palmichin, all of the 18 launch sites included in the inventory were operational in 2019. Almost all sites are in the Northern Hemisphere, except for Māhia in New Zealand. Several sites lie close to the equator (Figure 3); rockets launched from these sites may emit into the tropical pipe, thus providing longer lifetimes of emitted species (Plumb, 1996).

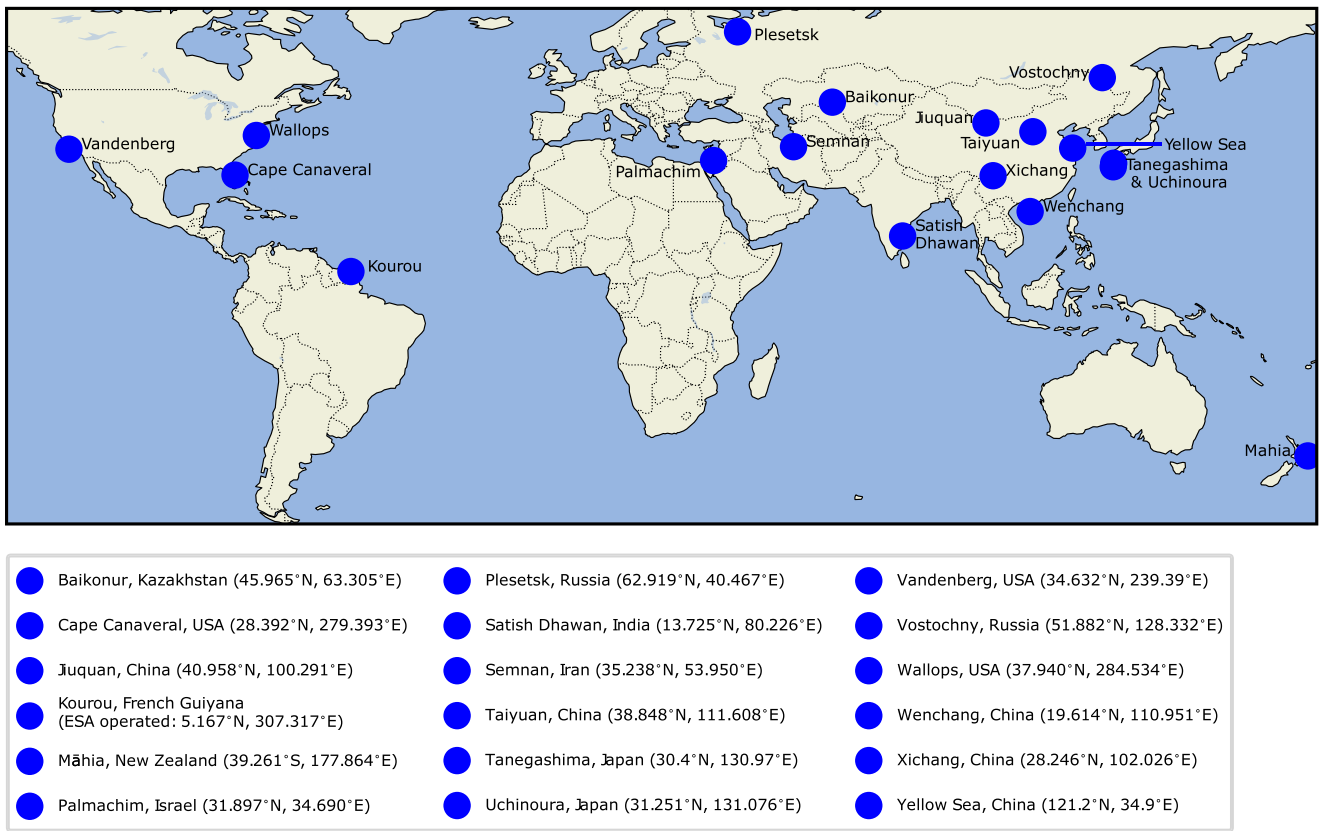

Figure 3. Launch sites included in the inventory. The country of operation is listed, with launch sites listed by colloquial naming. Note that the Kourou launch site is operated by the European Space Agency (ESA), and that Baikonur Cosmodrome in Kazakhstan is operated by Russia. In addition, no launches were carried out at Palmachim in 2019, so data for Israel are not included in the netCDF file. Relevant data for the vehicle (Shavit) operated at Palmachim are included in Tables 2–4 so that users may include it in modeling studies if they wish.

2.6. Comparison to Existing Inventories

The contemporary emissions inventories developed by Desain and Brady (2014) (launches from 1985 to 2013), Ryan et al. (2022) (launches in 2019), and Pradon et al. (2023) (launches from 2009 to 2018) are useful comparisons for this data set. Our methodology is most similar to that of Ryan et al. (2022), and thus we outline some specific differences for better understanding our inventory in context. In particular, we discuss our chain of assumptions leading from vehicle launch mass to stratospheric emissions explicitly at all points, to permit and improve reproducibility. This is key as much of this data is only semi-public, in commercial documents. Not all of these steps are given in other inventories.

Our choices of launch inclusion are outlined in Section 2, comprising 97 launches worldwide. Ryan et al. (2022) outline 103 launches for 2019, including all orbital launches regardless of outcome (including both launchpad failure, which we exclude, and failure to reach target orbit; see Section 2). They use a slightly different site naming convention, though the geographical coordinates are the same (e.g., Kagoshima vs. Uchinoura). Pradon et al. (2023) cover 77% of the launches between 2009 and 2018 in their modeling, including most large vehicles but omitting many of the smaller vehicles which we include. Furthermore, they entirely omit launches which occur in the Southern Hemisphere. While only 4 launches took place in the Southern Hemisphere during this period, this has increased by more than a factor of 10 since 2019, pointing to the importance of including geo-located Southern Hemisphere rocket launch emissions for future modeling studies.

Similar to Desain and Brady (2014), our inventory explicitly details stratospheric emissions, that is, the emission species per vehicle (Table 2). This is not present in the other two comparison inventories. Furthermore, Pradon et al. (2023) do not explicitly estimate black carbon emissions. Our inventory uses per-vehicle engine ignition and cut-off altitudes (burn profiles), outlined in Section 2.5, with the input file describing emissions production per

1 km altitude. Pradon et al. (2023) models burn profiles more comprehensively, but for only a subset of these vehicles. Ryan et al. (2022) uses the burn profile from Ross and Sheaffer (2014), which is extrapolated from a limited section of U.S.-based launches without SRM boosters, at 5 km increments, to all of their 103 launches.

These inventories have broad comparability, but small disparities are also seen in calculation of the proportion of fuel types burned in 2019. Ryan et al. (2022) estimate 45% kerosene, 32% hypergolic, 14% solid, and 8% liquid hydrogen makeup. In contrast, our inventory consists of 48% kerosene, 30% hypergolic, 16% solid, and 6% cryogenic fuel by total propellant burned across all launches (Table 1). We note that our inventory does not include later stages of launch vehicles, which are considerably less massive, but overwhelmingly hypergolic or cryogenic fuels.

The inventory is designed for use in global models. The resulting model output—for example, simulated impacts on the ozone layer—will be a function of different uncertainties (Gettelman & Rood, 2016). First, boundary condition uncertainty (here the choice of rocket launch emissions inventory): differences and similarities between our inventory and others are discussed above. Second, model uncertainty: for example, the type of model, level of detail in the model (e.g., number of species and reactions involved in the chemistry scheme) and biases in the model with respect to observations. Third, scenario uncertainty: the number of assumed future launches, and background concentrations of other species relevant to the ozone layer (e.g., greenhouse gases and ozone depleting substances). All three types of uncertainty will influence the simulated response of atmospheric composition and dynamics to rocket launch emissions. To overcome these uncertainties, many more studies are needed to simulate rocket launch emissions. Future work may investigate a multi-model intercomparison effort as has been done in the past via the Chemistry-Climate Model Initiative, as one such example (Morgenstern et al., 2017).

To provide more context for researchers looking to implement the inventory in their models, the next section provides guidance notes for users.

3. Guidance in Use of the Inventory in Modeling Studies

A subset of the inventory—the worldwide rocket emissions from successful launches that occurred in 2019—is freely available in netCDF format and designed to be easily used by global atmospheric models. These models simulate the response of Earth's atmosphere over a user-specified time period, which can include the future. The netCDF file provides a set of rocket launch emissions that can be added as an extra forcing, or scaled up to create a future scenario, to see how Earth's atmosphere responds with their additional presence. The netCDF file is available for download: see Section 5. It contains emissions for each vehicle at the geographical coordinates for which those vehicles are active (Figure 3). The netCDF has $1° \times 1°$ horizontal resolution and 1 km vertical resolution up to 80 km. The netCDF is also time-dependent, with monthly emission aggregates. All six emission species (water vapor, carbon dioxide, alumina, black carbon, Cl_x and NO_x) are included, geolocated to launch site. Emissions species are included as separate variables in the input file, with non-zero data occurring only at launch site coordinates.

The total launch site emissions, for example, could be calculated on a monthly basis by summing the entire altitude regime (1–80 km). Global emissions are calculated similarly, by summing all launch sites. For a per-vehicle scenario, users can leverage Table 2 for stratospheric-only calculations. Otherwise, per-vehicle scenarios can be built from scratch using Tables 4–6 for raw propellant and altitude data, multiplied by the emission indices in Table 8.

Future launch conditions can be easily extrapolated using both the netCDF input file and the tables listed in the main text, depending on user intention. A combination of these sources could create many adjusted launch scenarios based on vehicle prevalence, launch site traffic, or creation of new spaceports using the coordinate dimensions. Unlike single-emission stratospheric scenarios, using this data set will also allow users to preserve the ensemble nature and emission proportions of rocket launch emissions. Modeling the impacts of all propellants in combination will be important as stratospheric chemistry is non-linear: the combined impacts of multiple emissions products may be greater than its parts (Revell et al., 2015; Shindell & Grewe, 2002).

When using or adjusting this inventory, a few areas of uncertainty are important to understand. Principally, the inventory represents all active launch vehicles in 2019, all flight profiles and all species. This means it does not include newer launch vehicles or newer fuel types, such as liquid natural gas (LNG) fuel. These are a large source

of uncertainty in the aerospace industry, which could alter future scenarios. To a lesser extent, hypergolic fuels are beginning to see a decline in usage, with kerosene and LNG, which is predominantly methane, becoming more ubiquitous (most often for early vehicle stages). Users could add emissions to this data set to include newer vehicles—such as the iodine electric propulsion system modeled by Feng et al. (2023), which may cause stratospheric ozone depletion, and vehicles using LNG fuel, such as the SpaceX Starship. This vehicle is five times larger than the median vehicle (by propellant mass) in our inventory. We do not include it here as it did not launch in 2019, and its fuel type emission products are yet to be confirmed (SpaceX, 2022). However, for vehicles in this size class, even an infrequent launch cadence could have substantial effects on the global emissions.

This inventory is intended as a stand-alone benchmark for 2019. Future work may involve updating the inventory with new propellants as their emissions products become available, or extending it forward to cover more recent years with pandemic-modified launch schedules. We welcome user contributions and feedback. Changes to vehicle usage, fuel usage, or understanding of emission indices based on new research requires more involved user additions to the inventory, but may follow the same methodology. For instance, users may wish to contribute 50–80 km data from other sources, such as from ablated satellites (Schulz & Glassmeier, 2021). We highlight a use case specifically in the case of alumina in Section 2.4.

4. Conclusions

Frequent and sustained future rocket launches may jeopardize some of the gains achieved through the Montreal Protocol for Substances that Deplete the Ozone Layer and its amendments and adjustments. We anticipate it will provide significant benefit to the community to understand the potential future impacts of rocket launches. Here we have presented a current inventory of stratospheric emission products from global rocket launches, formatted for use in global chemistry-climate or Earth system models. The emissions inventory includes vehicle data and granular flight profiles for every orbital launch system used for 2019, and encompasses the four major fuel types currently in use (liquid kerosene, cryogenic, hypergolic, and solid). The inventory presents a global snapshot of current launch activity, providing a data set with which to explore potential future emission scenarios. We invite modeling groups to use our inventory, in combination with constructed scenarios of future launches, to answer pressing questions about the impacts of rocket emissions on 21st-century stratospheric ozone and climate.

Data Availability Statement

The full, model-ready input data files for global launches in 2019, emissions inventory tables, and vehicle-specific references for the data set are available at Brown (2024); https://zenodo.org/doi/10.5281/zenodo.6499776. The data on which this article is based are available in European Space Agency (2022), Space Launch Report (2022), Space Launch Report (2021, 2022b, 2017b, 2017a, 2022a, 2020), Stephen Clark (2020, 2017), Andrew Jones (2020), Mitsubishi Heavy Industries (2022), China Great Wall Industry Corporation (2010, 2022), China Space Report (2022), Mark Wade (2019), Japan Aerospace Exploration Agency (JAXA) and Mitsubishi Heavy Industries (2022), Gunter D. Krebs (2022), Robert A. Braeunig (2008), Russian Ministry of Defense (2014), Indian Space Research Organization (2022a, 2022b), Sutton and Biblarz (2001), United Launch Alliance (2013), China Academy of Launch Vehicle Technology (1999), China Great Wall Industry Corporation (2011), National Aeronautics and Space Administration (2014), United Launch Alliance (2010), Rocket Lab (2020), Arianespace (2012), International Launch Services (2009), Northrop Grumman (2016, 2020), Mitsubishi Heavy Industries Launch Services (2015), SpaceX (2021), Japanese Aerospace Exploration Agency (JAXA) (2018), ArianeSpace (2014), iSpace (2022), EURockot (2011).

Acknowledgments
TFMB received financial support from the University of Canterbury. MTB and LER appreciate support by the Rutherford Discovery Fellowships (UOC2001 and UOC2214) from New Zealand Government funding, administered by the Royal Society Te Apārangi. TS and ER were supported by the Swiss National Science Foundation (SNSF) (POLE (Grant 200020-182239)). We thank the anonymous reviewers for their helpful and thoughtful comments, and Jonathan McDowell for his space launch data-collection services for the community. MTB and LER thank Martin Ross and Leonard David for their Scientific American article (November 2020), "An Underappreciated Danger of the New Space Age: Global Air Pollution," which sparked the curiosity that led to this research. Open access publishing facilitated by $INSTITUTION, as part of the Wiley - $INSTITUTION agreement via the Council of Australian University Librarians.

References

Andrew Jones. (2020). Galactic energy prepares Ceres-1 rocket for first launch [Dataset]. https://spectrum.ieee.org/galactic-energy-prepares-ceres1-rocket-first-launch

ArianeSpace. (2012). Soyuz user's manual issue 2 revision 0 [Manual] [Dataset]. Retrieved from https://www.academia.edu/23456530/Soyuz_Users_Manual_March

ArianeSpace. (2014). Vega user's manual issue 4 revision 0 [Manual] [Dataset]. Retrieved from https://web.archive.org/web/20241007205252/https:/www.arianespace.com/wp-content/uploads/2018/05/Vega-Users-Manual_Issue-04_April-2014.pdf

Ban-Weiss, G. A., Cao, L., Bala, G., & Caldeira, K. (2012). Dependence of climate forcing and response on the altitude of black carbon aerosols. *Climate Dynamics*, *38*(5), 897–911. https://doi.org/10.1007/s00382-011-1052-y

Boley, A. C., & Byers, M. (2021). Satellite mega-constellations create risks in low earth orbit, the atmosphere and on earth. *Scientific Reports*, *11*(1), 10642. https://doi.org/10.1038/s41598-021-89909-7

Braeunig, R. A. (2008). Rocket propellants [Dataset]. http://www.braeunig.us/space/propel.htm
Brooke, J. S. A., Feng, W., Carrillo-Sánchez, J. D., Mann, G. W., James, A. D., Bardeen, C. G., et al. (2017). Meteoric smoke deposition in the polar regions: A comparison of measurements with global atmospheric models. *Journal of Geophysical Research: Atmospheres*, *122*(20), 11112–11130. https://doi.org/10.1002/2017JD027143
Brown, T. F. M. (2024). Rocket launch emission 2019 dataset [Dataset]. *Zenodo*. https://doi.org/10.5281/zenodo.6499776
Brown, T. F. M., Bannister, M. T., & Revell, L. E. (2023). Envisioning a sustainable future for space launches: A review of current research and policy. *Journal of the Royal Society of New Zealand*, *54*(3), 1–17. https://doi.org/10.1080/03036758.2022.2152467
Carpenter, L., Daniel, J., Fleming, E., Hanaoka, T., Hu, J., Ravishankara, A., et al. (2018). Scenarios and information for policymakers, Chapter 6 in scientific assessment of ozone depletion: 2018.
Carrillo-Sánchez, J. D., Gómez-Martín, J. C., Bones, D. L., Nesvorný, D., Pokorný, P., Benna, M., et al. (2020). Cosmic dust fluxes in the atmospheres of Earth, Mars, and Venus. *Icarus*, *335*, 113395. https://doi.org/10.1016/j.icarus.2019.113395
China Academy of Launch Vehicle Technology. (1999). LM-2C user's manual [Manual] [Dataset]. https://www.globalsecurity.org/space/library/report/1999/2c.htm
China Great Wall Industry Corporation. (2010). Long March 2D [Dataset]. http://www.cgwic.com/LaunchServices/LaunchVehicle/LM2D.html
China Great Wall Industry Corporation. (2011). LM-3A series launch vehicle user's manual [Manual] [Dataset]. https://www.cgwic.com/
China Great Wall Industry Corporation. (2022). Long March 2C [Dataset]. http://cgwic.com/Launchservice/LM2C.html
China Space Report. (2022). Chang Zheng 7 (Long March 7) [Dataset]. https://chinaspacereport.wordpress.com/launch-vehicles/cz7/
Crutzen, P. J. (1970). The influence of nitrogen oxides on the atmospheric ozone content. *Quarterly Journal of the Royal Meteorological Society*, *96*(408), 320–325. https://doi.org/10.1002/qj.49709640815
Dallas, J. A., Raval, S., Alvarez Gaitan, J. P., Saydam, S., & Dempster, A. G. (2020). The environmental impact of emissions from space launches: A comprehensive review. *Journal of Cleaner Production*, *255*, 120209. https://doi.org/10.1016/j.jclepro.2020.120209
Daniel, J. S., & Reimann, S. (2022). Scenarios and information for policymakers. In *Scientific assessment of ozone depletion: 2022. GAW report No. 278* (p. 509). WMO Scientific Assessment of Ozone Depletion: 2022. Chapter 7.
Danilin, M. Y., Ko, M. K. W., & Weisenstein, D. K. (2001). Global implications of ozone loss in a space shuttle wake. *Journal of Geophysics Research*, *106*(D4), 3591–3601. https://doi.org/10.1029/2000JD900632
Danilin, M. Y., Shia, R. L., Ko, M. K. W., Weisenstein, D. K., Sze, N. D., Lamb, J. J., et al. (2001). Global stratospheric effects of the alumina emissions by solid-fueled rocket motors. *Journal of Geophysics Research*, *106*(D12), 12727–12738. https://doi.org/10.1029/2001JD900022
Desain, J., & Brady, B. (2014). *Potential atmospheric impact generated by space launches worldwide—Update for emission estimates from 1985 to 2013 (Tech. Rep.). El Segundo*. The Aerospace Corporation. Retrieved from https://www.researchgate.net/publication/235802139_Potential_Atmospheric_Impact_Generated_by_Space_Launches_Worldwide_Update_for_Emission_Estimates_from_1985_to_2011
Dhomse, S. S., Kinnison, D., Chipperfield, M. P., Salawitch, R. J., Cionni, I., Hegglin, M. I., et al. (2018). Estimates of ozone return dates from Chemistry-Climate Model Initiative simulations. *Atmospheric Chemistry and Physics*, *18*(11), 8409–8438. https://doi.org/10.5194/acp-18-8409-2018
Dykema, J. A., Keith, D. W., & Keutsch, F. N. (2016). Improved aerosol radiative properties as a foundation for solar geoengineering risk assessment. *Geophysical Research Letters*, *43*(14), 7758–7766. https://doi.org/10.1002/2016GL069258
EURockot. (2011). Rockot user's guide [Manual] [Dataset]. http://www.eurockot.com/wp-content/uploads/2012/10/UsersGuideIss5Rev0web.pdf
European Space Agency. (2022). Boosters (EAP) [Dataset]. https://www.esa.int/Enabling_Support/Space_Transportation/Launch_vehicles/Boosters_EAP
Evan, S., Brioude, J., Rosenlof, K. H., Gao, R.-S., Portmann, R. W., Zhu, Y., et al. (2023). Rapid ozone depletion after humidification of the stratosphere by the Hunga Tonga eruption. *Science*, *382*(6668), eadg2551. https://doi.org/10.1126/science.adg2551
Farman, J. C., Gardiner, B. G., & Shanklin, J. D. (1985). Large losses of total ozone in Antarctica reveal seasonal ClOx/NOx interaction. *Nature*, *315*(6016), 207–210. https://doi.org/10.1038/315207a0
Feng, W., Plane, J. M. C., Chipperfield, M. P., Saiz-Lopez, A., & Booth, J.-P. (2023). Potential stratospheric ozone depletion due to iodine injection from small satellites. *Geophysical Research Letters*, *50*(7), e2022GL102300. https://doi.org/10.1029/2022GL102300
Gettelman, A., & Rood, R. B. (2016). *Demystifying climate models*. Springer Open.
Indian Space Research Organization. (2022a). GSLV Mk III [Dataset]. Retrieved from https://web.archive.org/web/20220319184147/https://www.isro.gov.in/launchers/gslv-mk-iii
Indian Space Research Organization. (2022b). Polar satellite launch vehicle [Dataset]. Retrieved from http://web.archive.org/web/20220107160349/https://www.isro.gov.in/launchers/pslv
International Launch Services. (2009). Proton launch system mission Planner's guide [Dataset]. The Manual. Retrieved from https://www.ilslaunch.com/launch-services/proton-mission-planners-guide/
iSpace. (2022). Hyperbola-1 user manual [Manual] [Dataset]. http://www.i-space.com.cn/statics/ispace/doc/Hyperbola-1%20User%20Manual.pdf
Jackman, C. H., Considine, D. B., & Fleming, E. L. (1996). Space shuttle's impact on the stratosphere: An update. *Journal of Geophysics Research*, *101*(D7), 12523–12529. https://doi.org/10.1029/96JD00577
Jackman, C. H., Considine, D. B., & Fleming, E. L. (1998). A global modeling study of solid rocket aluminum oxide emission effects on stratospheric ozone. *Geophysical Research Letters*, *25*(6), 907–910. https://doi.org/10.1029/98GL00403
Japan Aerospace Exploration Agency (JAXA) and Mitsubishi Heavy Industries. (2022). H-IIB launch vehicle No. 3 (H-IIB F3) overview [Dataset]. https://global.jaxa.jp/countdown/h2bf3/pdf/h2bf3_presskit_e.pdf
Japanese Aerospace Exploration Agency (JAXA). (2018). Epsilon launch vehicle user's manual [Manual] [Dataset]. https://global.jaxa.jp/projects/rockets/epsilon/pdf/EpsilonUsersManual_e.pdf
Karol, I. L., Ozolin, Y. E., & Rozanov, E. V. (1992). Effect of space rocket launches on ozone. *Annales Geophysicae*, *10*(10), 810–814. Retrieved from https://ui.adsabs.harvard.edu/abs/1992AnGeo.10.810K
Kim, S., Jo, B.-U., Choi, E.-J., Cho, S., & Ahn, J. (2019). Two-phase framework for footprint prediction of space object reentry. *Advances in Space Research*, *64*(4), 824–835. https://doi.org/10.1016/j.asr.2019.05.023
Kim, Y., Lee, H.-J., & Roh, T.-S. (2021). Analysis of propellant weight under re-entry conditions for a reusable launch vehicle using retro-propulsion. *Energies*, *14*(11), 3210. https://doi.org/10.3390/en14113210
Kravitz, B., Robock, A., Shindell, D. T., & Miller, M. A. (2012). Sensitivity of stratospheric geoengineering with black carbon to aerosol size and altitude of injection. *Journal of Geophysical Research*, *117*(D9). https://doi.org/10.1029/2011JD017341
Krebs, G. D. (2022). Launch vehicles, Gunter's space page [Dataset]. https://space.skyrocket.de/directories/launcher.htm
Larson, E. J. L., Portmann, R. W., Rosenlof, K. H., Fahey, D. W., Daniel, J. S., & Ross, M. N. (2017). Global atmospheric response to emissions from a proposed reusable space launch system. *Earth's Future*, *5*(5), 37–48. https://doi.org/10.1002/2016EF000399

Maloney, C. M., Portmann, R. W., Ross, M. N., & Rosenlof, K. H. (2022). The climate and ozone impacts of black carbon emissions from global rocket launches. *Journal of Geophysical Research: Atmospheres*, *127*(12), e2021JD036373. https://doi.org/10.1029/2021JD036373
Mark Wade. (2019). Encyclopedia Astronautica [Dataset]. http://www.astronautix.com/
McDowell, J. (2022). Jonathan's space report. https://www.planet4589.org/space/index.html
Mills, M. J., Toon, O. B., Turco, R. P., Kinnison, D. E., & Garcia, R. R. (2008). Massive global ozone loss predicted following regional nuclear conflict. *Proceedings of the National Academy of Sciences*, *105*(14), 5307–5312. https://doi.org/10.1073/pnas.0710058105
Mitsubishi Heavy Industries. (2022). MHI launch services: Launch vehicles [Dataset]. https://www.mhi.com/products/space/launch_srv_lineup.html
Mitsubishi Heavy Industries Launch Services. (2015). H-IIA user's manual [Manual] [Dataset]. https://www.mhi.com/jp/products/pdf/manual.pdf
Molina, M. J., Molina, L. T., Zhang, R., Meads, R. F., & Spencer, D. D. (1997). The reaction of $ClONO_2$ with HCl on aluminum oxide. *Geophysical Research Letters*, *24*(13), 1619–1622. https://doi.org/10.1029/97GL01560
Molina, M. J., & Rowland, F. S. (1974). Stratospheric sink for chlorofluoromethanes: Chlorine atom-catalysed destruction of ozone. *Nature*, *249*(5460), 810–812. https://doi.org/10.1038/249810a0
Morgenstern, O., Hegglin, M. I., Rozanov, E., O'Connor, F. M., Abraham, N. L., Akiyoshi, H., et al. (2017). Review of the global models used within phase 1 of the chemistry–climate model initiative (CCMI). *Geoscientific Model Development*, *10*(2), 639–671. https://doi.org/10.5194/gmd-10-639-2017
Murphy, D. M., Abou-Ghanem, M., Cziczo, D. J., Froyd, K. D., Jacquot, J., Lawler, M. J., et al. (2023). Metals from spacecraft reentry in stratospheric aerosol particles. *Proceedings of the National Academy of Sciences*, *120*(43), e2313374120. https://doi.org/10.1073/pnas.2313374120
Murray, N., Bekki, S., Toumi, R., & Soares, T. (2013). On the uncertainties in assessing the atmospheric effects of launchers. *EUCASS Proceedings Series*, *4*, 671–688. https://doi.org/10.1051/eucass/201304671
National Aeronautics and Space Administration. (2014). Orbital-2 mission to the international space station: Media press kit [Dataset]. https://www.nasa.gov/sites/default/files/files/Orb2_PRESS_KIT.pdf
Northrop, G. (2016). Propulsion products catalog: Castor motor series [Manual] [Dataset]. https://www.northropgrumman.com/wp-content/uploads/NG-Propulsion-Products-Catalog.pdf
Northrop Grumman. (2020). Antares data sheet [Manual] [Dataset]. https://www.northropgrumman.com/wp-content/uploads/DS18012_Antares_081120-1.pdf
Park, C., & Rakich, J. V. (1980). Equivalent-cone calculation of nitric oxide production rate during space shuttle re-entry. *Atmospheric Environment*, *14*(8), 971–972. https://doi.org/10.1016/0004-6981(80)90011-6
Park, S.-H., Navarro Laboulais, J., Leyland, P., & Mischler, S. (2021). Re-entry survival analysis and ground risk assessment of space debris considering by-products generation. *Acta Astronautica*, *179*, 604–618. https://doi.org/10.1016/j.actaastro.2020.09.034
Plumb, R. A. (1996). A "tropical pipe" model of stratospheric transport. *Journal of Geophysical Research*, *101*(D2), 3957–3972. https://doi.org/10.1029/95JD03002
Popp, P. J., Ridley, B. A., Neuman, J. A., Avallone, L. M., Toohey, D. W., Zittel, P. F., et al. (2002). The emission and chemistry of reactive nitrogen species in the plume of an Athena II solid-fuel rocket motor. *Geophysics Research Letters*, *29*(18), 1887. https://doi.org/10.1029/2002GL015197
Portmann, R. W., Daniel, J. S., & Ravishankara, A. R. (2012). Stratospheric ozone depletion due to nitrous oxide: Influences of other gases. *Philosophical Transactions: Biological Science*, *367*(1593), 1256–1264. https://doi.org/10.1098/rstb.2011.0377
Pradon, C. V. M., Eastham, S. D., Chossière, G., Sabnis, J., Speth, R. L., Barrett, S. R. H., & André Jooste, J. (2023). Global three-dimensional emission inventory for launch vehicles from 2009 to 2018. *Journal of Spacecraft and Rockets*, *60*(3), 716–727. https://doi.org/10.2514/1.A35385
Prather, M. J., Garcia, M. M., Douglass, A. R., Jackman, C. H., Ko, M. K. W., & Sze, N. D. (1990). The space shuttle's impact on the stratosphere. *Journal of Geophysical Research*, *95*(D11), 18583–18590. https://doi.org/10.1029/JD095iD11p18583
Randel, W. J., Wu, F., Russell III, J. M., Waters, J. W., & Froidevaux, L. (1995). Ozone and temperature changes in the stratosphere following the eruption of Mount Pinatubo. *Journal of Geophysical Research*, *100*(D8), 16753–16764. https://doi.org/10.1029/95JD01001
Ravishankara, A. R., Daniel, J. S., & Portmann, R. W. (2009). Nitrous oxide (N_2O): The dominant ozone-depleting substance emitted in the 21st century. *Science*, *326*(5949), 123–125. https://doi.org/10.1126/science.1176985
Revell, L. E., Bodeker, G. E., Huck, P. E., Williamson, B. E., & Rozanov, E. (2012). The sensitivity of stratospheric ozone changes through the 21st century to N_2O and CH_4. *Atmospheric Chemistry and Physics*, *12*(23), 11309–11317. https://doi.org/10.5194/acp-12-11309-2012
Revell, L. E., Tummon, F., Salawitch, R. J., Stenke, A., & Peter, T. (2015). The changing ozone depletion potential of N_2O in a future climate. *Geophysical Research Letters*, *42*(22), 10047–10055. https://doi.org/10.1002/2015GL065702
Rocket, L. (2020). Launch: Payload user's guide: Version 6.5 [Manual] [Dataset]. https://www.rocketlabusa.com/assets/Uploads/Rocket-Lab-Launch-Payload-Users-Guide-6.5.pdf
Ross, M. N., Danilin, M. Y., Weisenstein, D. K., & Ko, M. K. W. (2004). Ozone depletion caused by NO and H_2O emissions from hydrazine-fueled rockets. *Journal of Geophysical Research*, *109*(D21). https://doi.org/10.1029/2003JD004370
Ross, M. N., & Jones, K. L. (2022). Implications of a growing spaceflight industry: Climate change. *Journal of Space Safety Engineering*, *9*(3), 469–477. https://doi.org/10.1016/j.jsse.2022.04.004
Ross, M. N., Mills, M., & Toohey, D. (2010). Potential climate impact of black carbon emitted by rockets. *Geophysical Research Letters*, *37*(24), 1–6. https://doi.org/10.1029/2010GL044548
Ross, M. N., & Sheaffer, P. M. (2014). Radiative forcing caused by rocket engine emissions. *Earth's Future*, *2*(4), 177–196. https://doi.org/10.1002/2013ef000160
Ross, M. N., Toohey, D. W., Rawlins, W. T., Richard, E. C., Kelly, K. K., Tuck, A. F., et al. (2000). Observation of stratospheric ozone depletion associated with Delta II rocket emissions. *Geophysics Research Letters*, *27*(15), 2209–2212. https://doi.org/10.1029/1999GL011159
Russian Ministry of Defense. (2014). Simulation of the launch of the Angara-A5 ILV and the launch of the payload into orbit [Dataset]. https://www.youtube.com/watch?v=TuzZ5mVljq8
Ryan, R. G., Marais, E. A., Balhatchet, C. J., & Eastham, S. D. (2022). Impact of rocket launch and space debris air pollutant emissions on stratospheric ozone and global climate. *Earth's Future*, *10*(6), e2021EF002612. https://doi.org/10.1029/2021EF002612
Schmid, O., Reeves, J. M., Wilson, J. C., Wiedinmyer, C., Brock, C. A., Toohey, D. W., et al. (2003). Size-resolved particle emission indices in the stratospheric plume of an Athena II rocket. *Journal of Geophysical Research (Atmospheres)*, *108*(D8), 4250. https://doi.org/10.1029/2002JD002486

Schulz, L., & Glassmeier, K.-H. (2021). On the anthropogenic and natural injection of matter into earth's atmosphere. *Advances in Space Research*, *67*(3), 1002–1025. https://doi.org/10.1016/j.asr.2020.10.036

Sheaffer, P. M. (2021). Garbage-in garbage-out (GIGO): The use and abuse of combustion modeling and recent U.S. Spacelaunch environmental impacts. *AGU 2021 Fall Meeting (via ESSOAR)*, *18*. https://doi.org/10.1002/essoar.10509138.9

Shindell, D. T., & Grewe, V. (2002). Separating the influence of halogen and climate changes on ozone recovery in the upper stratosphere. *Journal of Geophysical Research*, *107*(D12). ACL 3-1-ACL 3-10. https://doi.org/10.1029/2001JD000420

Solomon, S. (1999). Stratospheric ozone depletion: A review of concepts and history. *Reviews of Geophysics*, *37*(3), 275–316. https://doi.org/10.1029/1999RG900008

Solomon, S., Stone, K., Yu, P., Murphy, D. M., Kinnison, D., Ravishankara, A. R., & Wang, P. (2023). Chlorine activation and enhanced ozone depletion induced by wildfire aerosol. *Nature*, *615*(7951), 259–264. https://doi.org/10.1038/s41586-022-05683-0

Space Launch Report. (2022). Antares specifications [Dataset]. Retrieved from https://launchreport.neocities.org/antsum.txt

Space Launch Report. (2017a). H-IIA/B data sheet [Dataset]. Retrieved from https://sma.nasa.gov/LaunchVehicle/assets/h-iiab-data-sheet.pdf

Space Launch Report. (2017b). Taurus data sheet [Dataset]. Retrieved from https://launchreport.neocities.org/mxsum.txt

Space Launch Report. (2020). Shavit data sheet [Dataset]. Retrieved from https://launchreport.neocities.org/shavsum.txt

Space Launch Report. (2021). Ariane 5 data sheet [Dataset]. Retrieved from https://launchreport.neocities.org/ariane5.txt

Space Launch Report. (2022a). Safir data sheet [Dataset]. Retrieved from https://launchreport.neocities.org/safrsum.txt

Space Launch Report. (2022b). Atlas 5 data sheet [Dataset]. Retrieved from https://launchreport.neocities.org/atl5sum.txt

SpaceX. (2021). Falcon user's guide [Manual] [Dataset]. https://www.spacex.com/media/falcon-users-guide-2021-09.pdf

SpaceX. (2022). SpaceX starship. https://www.spacex.com/vehicles/starship/

Stephen, C. (2017). Timeline of Minotaur-C launch with SkySats and Doves [Dataset]. https://spaceflightnow.com/2017/10/30/timeline-of-minotaur-c-launch-with-skysats-and-doves/

Stephen, C. (2020). Atlas 5 launch timeline for the AEHF 6 mission [Dataset]. https://spaceflightnow.com/2020/03/26/atlas-5-launch-timeline-for-the-aehf-6-mission/

Sutton, G. P., & Biblarz, O. (2001). *Rocket propulsion elements*. John Wiley & Sons.

Tian, W., Chipperfield, M. P., & Lü, D. (2009). Impact of increasing stratospheric water vapor on ozone depletion and temperature change. *Advances in Atmospheric Sciences*, *26*(3), 423–437. https://doi.org/10.1007/s00376-009-0423-3

United Launch Alliance. (2010). Atlas V launch services user's guide [Manual] [Dataset]. https://www.ulalaunch.com/docs/default-source/rockets/atlasvusersguide2010.pdf

United Launch Alliance. (2013). Delta IV launch services user's guide [Manual] [Dataset]. Retrieved from https://www.ulalaunch.com/docs/default-source/rockets/delta-iv-user's-guide.pdf

Voigt, C., Schumann, U., Graf, K., & Gottschaldt, K.-D. (2013). Impact of rocket exhaust plumes on atmospheric composition and climate—An overview. *Progress in Propulsion Physics*, *4*, 657–670. https://doi.org/10.1051/eucass/201304657

Weisenstein, D. K., Keith, D. W., & Dykema, J. A. (2015). Solar geoengineering using solid aerosol in the stratosphere. *Atmospheric Chemistry and Physics*, *15*(20), 11835–11859. https://doi.org/10.5194/acp-15-11835-2015

Yu, P., Toon, O., Bardeen, C., Zhu, Y., Rosenlof, K., Portmann, R., et al. (2019). Black carbon lofts wildfire smoke high into the stratosphere to form a persistent plume. *Science*, *365*(6453), 587–590. https://doi.org/10.1126/science.aax1748